LARGE EDDY SIMULATION OF NEAR-WALL TURBULENT FLOW OVER STREAMLINED RIBLET-STRUCTURED SURFACE FOR DRAG REDUCTION IN A RECTANGULAR CHANNEL

by

Hussain H. Al-KAYIEM**, Desmond C. LIM, and Jundika C. KURNIA

Mechanical Engineering Department, University Teknologi PETRONAS,
Bandar Seri Iskandar, Malaysia

Original scientific paper
https://doi.org/10.2298/TSCI190909059A

Sharkskin-inspired riblets are widely adopted as a passive method for drag reduction of flow over surfaces. In this research, large eddy simulation of turbulent flow over riblet-structured surface in a rectangular channel domain were performed at various Reynolds numbers, ranging from 4200-10000, to probe the resultant drag change, compared to smooth surface. The changes of mean streamwise velocity gradient in wall-normal direction at varied locations around riblet structures were also investigated to reduce mechanisms of streamlined riblet in reducing drag. The computational model is validated by comparing the simulation results against analytical and experimental data, for both smooth and riblet surfaces. Results indicating that the performance of the proposed streamlined riblet shows 7% drag reduction, as maximum, which is higher than the performance of L-shaped riblet with higher wetted surface area. The mean velocity profile analysis indicates that the streamlined riblet structures help to reduce longitudinal averaged velocity component rate in the normal to surface direction of near-wall region which leads to laminarization process as fluid-flows over riblet structures.

Key words: *drag reduction, large eddy simulation, near-wall velocity profile, streamlined riblet, turbulence control, turbulent channel flow*

Introduction

Drag reduction is an important topic in engineering field. Many investigations are conducted to optimize the drag of a travelling body for improvement of motion and energy consumption, especially in turbulent flow due to higher produced drag. In internal flow, such as channel and pipe flow, drag force is encountered at the bounded wall which ultimately leads to reduction of energy efficiency due to high pressure loss. The introduction of polymer additives into a flow system had seen its success of application since the discovery by [1], with reported drag reduction of around 80%. However, the additive-removal process, which requires extra energy input, often nullify the performance of total drag reduction. Hence, researchers explored the method of modifying surface morphology, in the attempt to produce drag reduction effect without additional energy consumption. Inspired by the fast travel speed of shark under water, the sharkskin and its scales are investigated, which then led to the introduction of riblet-structured surface. The sharkskin-inspired riblet structures are widely applied in turbulent flow studies and have shown positive drag reduction effect. The investigation by [2] suggested that

* Corresponding author, e-mail: hussain_kayiem@utp.edu.my

quasi-streamwise vortices are found in the near-wall region ($y^+ \leq 100$) and the presence of these vortices are associated with region of high turbulent stress, $\overline{u_i' u_j'}$ [3]. Following the findings, a mechanism for drag reduction was proposed, such that the restriction of interactions between the vortices would reduce the level of momentum exchange between high momentum fluid and low momentum fluid in the boundary-layer. As fluid-flows over the riblet structured-surfaces, the ribbed-shaped protrusions serve as *fence* that prohibit the lateral movement of coherent structures such as quasi-streamwise vortices in the turbulent boundary-layer [4-6]. By restricting the movement of the vortices, the level of momentum exchange can be reduced, which leads to drag reduction effect.

The common geometries of riblet structures investigated are *V*-shaped, *U*-shaped, and *L*-shaped with general range of 5-11% in terms of drag reduction performance [7-9]. The early works were conducted by [10, 11]. They proved the capability of *V*-groove riblet in producing drag reduction of 8%. Flow over segmented trapezoidal blade riblets (*L*-shaped) were investigated by [12] and produced drag reduction of 7.29%. [13] found that the highest drag reduction performance achieved by segmented *L*-shaped riblet was 5.2%. Despite being closer to shape of real sharkskin scale in terms of segmented-feature, the drag reduction performance of segmented riblet is found to be worse than the continuous riblet. It is suggested that the segmented gaps on real sharkskin may not help in reducing drag encountered but functions to eject the contaminant particles on sharkskin [12, 13]. One of the limitations imposed by riblet structure is the introduction of protrusions into the flow system, which increases the wetted surface area, despite achieving higher turbulent drag than skin-frictional drag in overall. This serves as one of the factors that hinder the progress of drag reduction performance by riblet structure.

However, simply reducing the wetted surface area may also result in loss of drag reduction capabilities of riblet structure, which leads to increased drag, since the modification of surface area will affect the riblet configuration and the turbulence structure near the internal wall of the channel. Based on the aforementioned findings, a morphology that is smaller in wetted surface area and capable of impedes the vortices interactions shall be proposed to improve the drag reduction performance of riblet structures. From the results reported by [14], it has been found that streamlined-shaped wing promotes laminar flow along the streamwise direction of flow. Another advantage of streamline feature of riblets is the reduction of wetted surface area. Therefore, it is of interest to integrate the streamlined feature in the design of riblet geometry, which is also yet to be found in other similar investigations.

In the current investigation, streamlined segmented-riblet structures were proposed to reduce the overall drag. The drag parameters of the proposed streamlined-riblet structure were investigated at Reynolds numbers of 4200, 6000, 8000, and 10000. In each flow case, the development of the velocity profiles around the riblet geometry was analyzed for insight understanding of flow dynamics around the riblets. The results are presented in such a way to establish insight understanding of the near-wall flow structure on the shearing drag in rectangular channel flow.

Numerical method

In their review paper on specific aspects of turbulent flow in rectangular ducts, [15] commented that respite over a century of research, turbulence remains the major unsolved problem of classical physics. While most researchers agree that the essential physics of turbulent flows can be described by the Navier-Stokes equations, limitations in computer capacity make it impossible – for now and the foreseeable future – to directly solve these equations in the complex turbulent flows of technological interest. Hence, virtually all scientific and engineering calculations of non-trivial turbulent flows, at high Reynolds numbers, are based on some type of modelling. This modelling can take a variety of forms.

Two basic levels of modelling currently used in CFD and transport processes are eddy viscosity models and second-moment closure models (known also as Reynolds stress models). Each category has a number of variants.

Turbulent flow over riblet structure is simulated by using numerical approach, since the turbulence phenomenon is chaotic and non-linear in nature. To capture the fluctuating turbulent statistics and drag parameters induced by turbulent energy dissipation of small scales more accurately, large eddy simulation (LES) is opted as it is an unsteady scale-resolving turbulence model. By assuming unsteady, incompressible flow with negligible effect of external energy and body force, the continuity and momentum equations are described, respectively:

$$\frac{\partial u_j}{\partial x_j}=0 \tag{1}$$

$$\frac{\partial u_i}{\partial t}+\frac{\partial}{\partial x_j}\left(u_i u_j\right)=-\frac{\partial P}{\partial x_i}+\frac{\partial}{\partial x_j}\left(\sigma_{ij}\right), \qquad i,j=1,2,3 \tag{2}$$

where x_j is the the spatial co-ordinates, t – the time, U – represents velocity, and P – the pressure.

The viscous stress tensor, σ_{ij} is defined:

$$\sigma_{ij}\equiv\left[\mu\left(\frac{\partial\overline{u_i}}{\partial x_j}+\frac{\partial\overline{u_j}}{\partial x_i}\right)\right]-\frac{2}{3}\mu\frac{\partial\overline{u_l}}{\partial x_l}\delta_{ij} \tag{3}$$

where dynamic viscosity is denoted by symbol μ, and δ_{ij} is the Kronecker delta.

In contrast to direct numerical simulation which solves the Navier-Stokes equations by resolving all time and length scales of flow field, LES reduces the computational effort by filtering out the small scales in the flow and model them to provide closure to the solution while the unfiltered large eddies are resolved directly. By applying filtering operations, the momentum equation becomes:

$$\frac{\partial u_i}{\partial t}+\frac{\partial}{\partial x_j}\left(u_i u_j\right)=-\frac{\partial P}{\partial x_i}+\frac{\partial}{\partial x_j}\left(\sigma_{ij}\right)+\frac{\partial}{\partial x_j}\left(\tau_{ij}\right) \tag{4}$$

The subgrid-scale stress, τ_{ij} is defined:

$$\tau_{ij}\equiv\rho\overline{u_i u_j}-\rho\bar{u}_i\bar{u}_j \tag{5}$$

The subgrid-scale turbulent stresses were computed, using subgrid-scale (SGS) model:

$$\tau_{ij}-\frac{1}{3}\tau_{kk}\delta_{ij}=-2\mu_t\overline{S_{ij}} \tag{6}$$

where μ_t is the subgrid-scale turbulent viscosity and τ_{kk} – the isotropic subgrid-scale stresses. The rate-of-strain tensor, $\overline{S}_{ij}$, is defined:

$$\overline{S_{ij}}=\frac{1}{2}\left(\frac{\partial\overline{u_i}}{\partial x_j}+\frac{\partial\overline{u_j}}{\partial x_i}\right) \tag{7}$$

and the turbulent viscosity, μ_t is modeled by Smagorinsky-Lilly model [16, 17]:

$$\mu_t=\rho L_s^{\,2}\left|\overline{S}\right| \tag{8}$$

where L_s is the mixing length, defined in detail by [17], which relates Smagorinsky coefficient and the grid filter scale, typically equal to the grid spacing, while $|\bar{S}| \equiv (2\bar{S}_{ij}\bar{S}_{ij})^{1/2}$. The commercial software package, ANSYS FLUENT is used as it adopts finite volume method, in which the entire domain is discretized into smaller volumes before solving the PDE in algebraic equations form. Least squares cell-based gradient is adopted for computation of convective terms and diffusive terms. Second order scheme is used for pressure interpolation at the faces. Bounded central-differencing scheme is adopted for momentum equation improve accuracy of LES calculation. The simulations were performed in high performance computer machine type Dell Precisionwer 7820, 20 cores, with the following specifications:

– Intel Xeon Silver 4116 2.1 GHz, 3.0 GHz Turbo, 12C, 9.6 GT/s 2UPI, 16MB Cache, HT (85W) DDR42400.
– Intel Xeon Silver 4116 2.1 GHz, 3.0 GHz Turbo, 12C, 9.6 GT/s 2UPI, 16M Cache, HT (85W) DDR42400 2nd.
– Boot drive or storage volume is greater than 2TB (select when 3TB/4TB HDD is ordered).
– Riser Card and Mid-Wall including Air shroud Cover for 2nd CPU module.
– 32 GB (4 × 8 GB) DDR4 2666 MHz RDIMM ECC.
– 2.5″ 256 GB SATA Class 20 Solid State Drive and 4 No. hard Drive.

The simulations took approximately ten days to reach statistically stable state and additional ten days for time averaging process.

Model description

Turbulent single-phase water was designed to flow through a rectangular channel with smooth wall as top surface and riblet structure as bottom surface. This allows direct comparison of drag change at smooth surface and riblet structure. The density and dynamic viscosity of water were taken as 1000 kg/m^3 and 0.001 kg/ms, respectively. The flow in streamwise, x_1-direction imposes a constant mass-flow rate:

$$\dot{m} = \rho \int U \mathrm{d}A = \frac{2}{3} \rho A_c U_c \tag{9}$$

where U_c is the centerline velocity of a laminar parabolic profile and A_c – the cross-sectional area of the rectangular channel. The average velocity is denoted by U and 2/3 of centerline velocity, U_c. Reynolds number is calculated based on laminar centerline velocity U_l and channel half-height, ($\delta = 0.5\,H$):

$$\mathrm{Re} = \frac{U_l \delta}{\nu} \tag{10}$$

For comparison of result against other published work, the dimensions of the fluid domain are non-dimensionalized by scale of u_τ/ν which can be written using a general variable, Φ:

$$\Phi^+ = \frac{\Phi\, u_\tau}{\nu} \tag{11}$$

where u_τ is the friction velocity and ν – the local kinematics viscosity of fluid (= 10^{-6} m^{2}s). The superscript, $^+$ is the non-dimensionalized parameters. The friction velocity is calculated:

$$u_\tau = \left(\frac{\tau_w}{\rho}\right)^{1/2} \tag{12}$$

where wall shear stress $\tau_w = (0.5\, C_f \rho U^2)$ estimated based on empirical formula of skin-friction coefficient, C_f, for channel flow of Reynolds number greater than 2800 [18], $C_f = 0.0376\mathrm{Re}^{-1/6}$.

However, the mesh is modified before activation of LES model such that wall shear stress, τ_w at the smooth surface of channel is obtained from steady-state simulation for higher accuracy, since LES simulation is highly sensitive towards mesh resolutions and qualities.

Computational domain

The schematic geometry of fluid domain is presented in fig. 1, where a cubic flow unit is used to represent the entire domain of numerical simulation. The solid aspect is neglected since it does not affect the solution of fluid-flow, which is the primary concern of current investigation. The flow is designed to pass through the stream-wise cross-sectional area ($A_c = HW$), where $H = 0.015$ m denotes the height of channel that describes the distance between smooth surface and riblet structure surface, and $W = 0.02$ m represents the channel width between two side surfaces. The length of channel in stream-wise direction is denoted by L in which three rows of riblets are arranged with equal gaps, L_1 in between. The isolation of basic flow unit for computational boxes is designed to be able to capture the flow dynamics and its effects on turbulence in fully developed flow. The proposed cubic fluid domain in current work is such that the dimensionless wall unit width in span-wise direction is approximately $W^+ \approx 400$ and the channel length in streamwise direction is approximately $L^+ \approx 400$ This allows accurate capture of turbulent structures and turbulent parameters of interest since the chosen flow unit is larger than the suggested minimal flow unit for computational boxes by [19], with wall unit of $z^+ \geq 100$ for spanwise width and $x^+ \geq 250$ for streamwise length. The riblet structure is a wall embedded with riblets protruded into the normal direction of wall. The configuration is such that the riblets are aligned-segmented in streamwise direction with spacing in span-wise direction between each riblet. Each riblet is proposed to be streamlined in the streamwise direction. The streamline feature is designed to help in reduction of drag encountered on the surface of riblets.

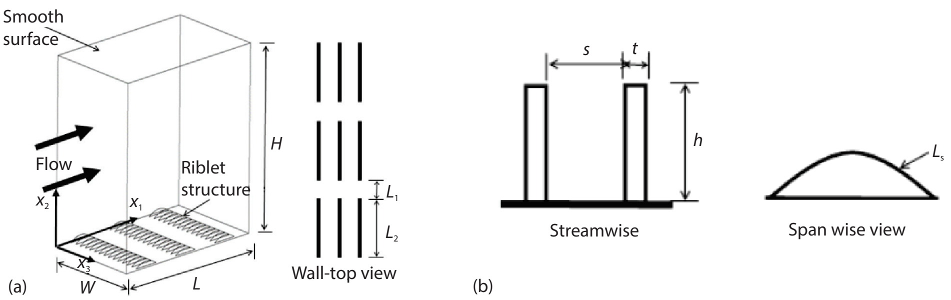

Figure 1. Computational domain description; (a) 3-D view of fluid domain, (b) cross-sectional view of riblet configuration

The channel height for the channel model is designed to be $H^+ = 375$. For simplification of design, a symmetrical convex-shaped streamline feature is chosen, whereby quadratic parabolic equation in the form, $L_s = -1/8L_2^2 + 2L_2$, is used to construct the streamline curve, L_s of riblets. The riblets are spaced by $s = 2$ mm in the spanwise direction. The inlet, outlet and side walls are defined as periodic boundary conditions to simulate fully developed flow in streamwise direction, with prescribed flow rate calculated by eq. (9). Both riblet-structured surface and smooth surface are prescribed with no-slip wall condition. The dimensions of riblet structures is presented in tab. 1. The dimensions are normalized by u_τ/ν as described by eq. (11), for comparison of results. The simulations were carried out for Reynolds number of 4200, 6000, 8000, and 10000 with the same configuration investigate the effect of flow parameters to drag change and turbulence parameters.

Table 1. Dimensions of the streamlined-riblet structure; superscript + denotes non-depersonalization of parameters by using eq. (11)

Re	s^+	h^+	t^+	L_1^+	L_2^+	h^+/s^+	t^+/s^+	L_2^+/L_1^+
4200	19.0	9.5	0.4	75.8	75.8	0.5	0.02	1
6000	26.3	13.1	0.5	105.1	105.1	0.5	0.02	1
8000	34.2	17.1	0.7	136.8	136.8	0.5	0.02	1
10000	42.0	21.0	0.8	167.8	167.8	0.5	0.02	1

The height to spacing ratio, h^+/s^+ is 0.5 across all cases, as this ratio was found to be the optimum configuration for drag reduction with riblet structures [6, 12]. Despite the change of dimensionless values with varied Reynolds numbers due to change of friction velocity, the ratios of the geometrical parameters remain consistent across various flow cases, based on tab. 1. This allows fair investigation of effect of flow parameter to the drag parameters. The thickness, t^+, length of riblet, L_2^+ and aligned-segmented gap between riblets, s^+ follows the configuration by [13] for comparison of drag reduction performance.

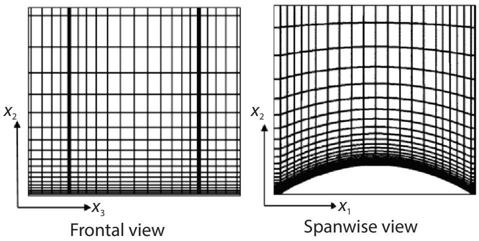

Figure 2. Computational mesh generated near the riblets, with hexahedral non-uniform mesh biased towards the boundary; mesh generated follows the parabolic profile of riblet streamline curve, in streamwise direction

Mesh generation

The entire fluid domain is discretized into hexahedral meshes to allow faster convergence rate and lesser computational effort as compared to full tetrahedral mesh. In the streamwise direction, a non-uniform mesh that biased towards riblet front and tail is used, with maximum mesh spacing of $x_1^+ = 5$, which is significantly smaller in spacing as compared to the mesh ($x_1^+ = 16$) adopted by [20]. In wall normal direction, non-uniform mesh is adopted since finer mesh must be generated at the near-wall region resolve the turbulent boundary-layer accurately.

The mesh resolution in wall normal direction near the riblet structures follows the parabolic distribution due to geometry of riblets. The first layer spacing, $x_2^+ = 0.2$ is adopted in current work which was sufficient to resolve viscous sublayer of the flow. The number of mesh in wall normal direction increases along with Reynolds numbers to maintain the x_2^+ requirement. In spanwise direction, mesh point of 225 is used with maximum spacing of $x_3^+ = 1.5$. The total mesh resolution of entire fluid domain is 120 × 66 × 225 in x_1-, x_2-, and x_3-direction, respectively, which is sufficient for simulating turbulence structure in a channel flow for LES simulation. To examine the influence of total mesh on the turbulence statistics, the mesh resolution in span-wise direction is doubled. The resultant drag change for case (Re = 4200) is less than 2%. Meaning to say that the doubled mesh resolution use in spanwise caused a reduction in the predicted drag value.

Drag parameters and turbulence statistics prediction

For each case, the simulations were started by running steady-state simulation with SST k-ω turbulence model, based on constant instantaneous laminar mass-flow rate in streamwise direction, as described in eq. (9). Turbulent intensity (TI) is imposed to the inlet surface of steady-state simulation:

$$TI = 0.14\,\mathrm{Re}_{D_H}^{-0.079} \tag{13}$$

to generate more realistic turbulence statistics for LES [21]. The instantaneous velocity, based on turbulent fluctuations in the flow, was then extracted from the steady flow to provide perturbation the inlet before activation of LES model. This helps to create a more realistic initial field for LES simulation and reduce the time consumption. The flow were simulated with LES model until it became statistically steady. This can be observed from the quasi-periodic behavior of resulted instantaneous drag on both riblet structure and smooth surface. The simulations were then continued for additional ($T^+ = 500$) non-dimensional time steps where $T^+ = TU_l/\delta$ to time-average the generated drag and resolved turbulent statistics.

Time-averaged drag

The instantaneous drag is calculated as integral of the product of wall shear stress and the differential wetted surface area, dA. In the designed flow cases, the protrusions of riblet structure introduce wetted surface area, normal to the streamwise direction,$(\hat{n}\cdot\hat{i})$. This leads to consideration of pressure drag, D_p in the calculation of total drag force, along with frictional drag, D_f which acts in tangential direction the streamwise direction, $(\hat{t}\cdot\hat{i})$. The computed drag forces are scaled by $0.5\rho U_b^2 A$, for comparison between smooth and riblet-structured surface, where ρ, U_b, and A are denoting density of fluid, bulk velocity and reference area, respectively. The non-dimensional drag coefficients, C_D, of smooth and riblet-structured surface are described:

$$C_{D\mathrm{smooth}} = \frac{2}{\rho U_b^2 A}\left[\underbrace{\mu\int\frac{\partial u_1}{\partial x_2}\left(\hat{t}\cdot\hat{i}\right)\mathrm{d}A_{\mathrm{smooth}}}_{D_{f\,\mathrm{smooth}}} + \underbrace{\int P\left(\hat{n}\cdot\hat{i}\right)\mathrm{d}A_{\mathrm{smooth}}}_{D_{p\mathrm{smooth}}}\right] \tag{14a}$$

$$C_{D\mathrm{riblet}} = \frac{2}{\rho U_b^2 A}\left[\underbrace{\mu\int\frac{\partial u_1}{\partial x_2}\left(\hat{t}\cdot\hat{i}\right)\mathrm{d}A_{\mathrm{riblet}}}_{D_{f\,\mathrm{riblet}}} + \underbrace{\int P\left(\hat{n}\cdot\hat{i}\right)\mathrm{d}A_{\mathrm{riblet}}}_{D_{p\mathrm{riblet}}}\right] \tag{14b}$$

where μ is the dynamic viscosity, while U and x_2 are the streamwise velocity and spatial co-ordinate in wall-normal direction, respectively. The drag reduction performance is obtained by comparison of computed drag change at the smooth surface and riblet structure. Since the channel flow is almost symmetric at the centerline, both surfaces act independently, and the drag change obtained is not affected by each other.

Mean-velocity prediction

The changes of mean streamwise velocity with respect to wall-normal direction, is investigated by obtaining time-averaged mean streamwise velocity, u_1 at different x_1 and x_3 co-ordinates. To investigate the development of velocity gradients around riblet structure, wall points are created at varied location along span-wise and streamwise direction, as shown in fig. 3.

The wall points are created along x_2-direction from surface ($x_2^+ = 0$) to the centerline ($x_2^+ \approx 0.5H^+$), for both smooth and riblet-structured surface, with same corresponding location mirrored by centerline. The number of points along x_2-direction is approximately 45 for respective surface, with smaller spatial interval between wall points at the near-wall region for better resolution of velocity gradient at the region.

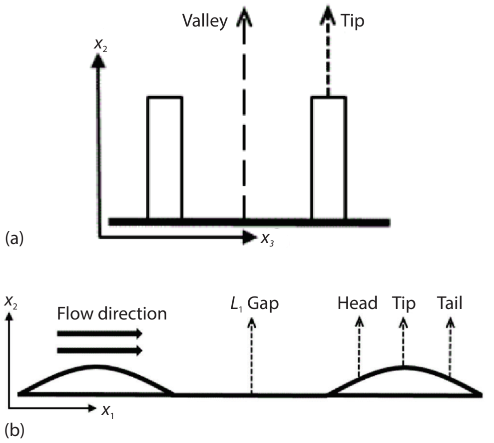

Figure 3. The locations of wall units in span-wise variation and streamwise variation; (a) frontal view, valley = 1/2 valley gap, tip = 1/2 riblet thickness, (b) spanwise view, L_1 gap = 1/2 L_1, head and tail = 1/2 L_2, tip = 1/2L_2

Results and discussions

Model validation

To examine the capability of LES model in current work, a rectangular channel flow over riblet structure is simulated. The chosen computational domain is shown in fig. 4, where continuous *L*-shaped riblet in streamwise direction is adopted, with similar configuration based on the riblet model investigated by [22].

The streamwise, span-wise and wall-normal directions are represented by x_1, x_2, x_3, respectively. The inlet and outlet boundary conditions are prescribed with translational periodic condition. The mass-flow rate in the streamwise direction is 0.111 kg/s, as calculated from eq. (9). This is corresponding to Reynolds number of 4180. The side walls are prescribed with symmetry condition whereas both riblet structure and smooth wall are set as with no-slip wall.

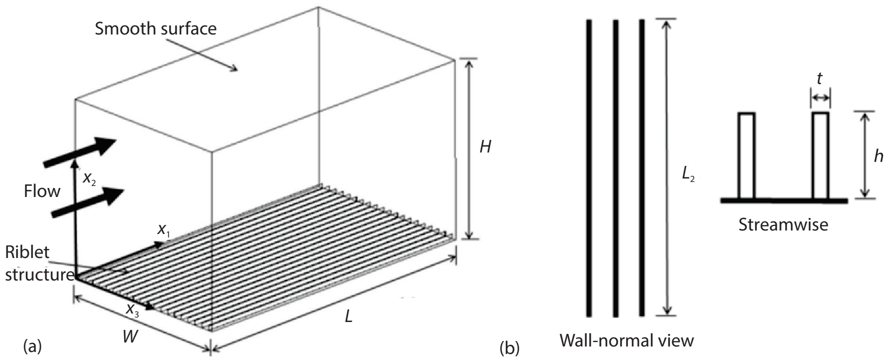

Figure 4. Computational domain for validation; (a) 3-D view of fluid domain, (b) cross-sectional view of riblet configuration

The computational mesh adopted was 35 × 92 × 297, in x_1-, x_2-, x_3-direction, respectively. The mesh in the wall-normal direction is biased towards the smooth wall and riblet structure. By following the simulation procedure mentioned in section *Numerical method*, the simulation is started by steady-state flow using SST k-ω turbulence model before LES-SGS model is enabled to run on initial field created by steady-state simulation, until the flow is statistically stable. The simulation is continued ($T^+ = 500$) to time-average the instantaneous drag resulted at both riblet structure and smooth wall

The validation results suggest that the LES model adopted is capable of capturing the drag parameters and mean velocity profile with acceptable accuracy. The validation results are presented in fig. 5. For comparison against analytical formula of law of wall, streamwise mean velocity, $\overline{u}_1$ is non-dimensionalized by simulated local friction velocity, u_τ such that $u^+ = \overline{u}_1/u_\tau$. For current study, Reichardt's Law of Wall [23] is adopted as comparison benchmark, since the corresponding formula is valid for all range of wall-normal height ($y^+ \geq 0$) and more convenient practically as compared to the other two-point formulas. By changing the representation of wall-co-ordinate, such that $y^+ \rightarrow x_2{}^+$, the formula of Reichardt's Law of Wall is described:

$$u^+ = 2.5\ln\left(1+0.4x_2{}^+\right)+7.8\left[1-\mathrm{e}^{-\frac{x_2{}^+}{11}}-\left(\frac{x_2{}^+}{11}\right)\mathrm{e}^{-0.33x_2{}^+}\right] \tag{15a}$$

Based on fig. 5(a), the mean velocity profile is in close agreement with the Reichardt's Law of Wall.

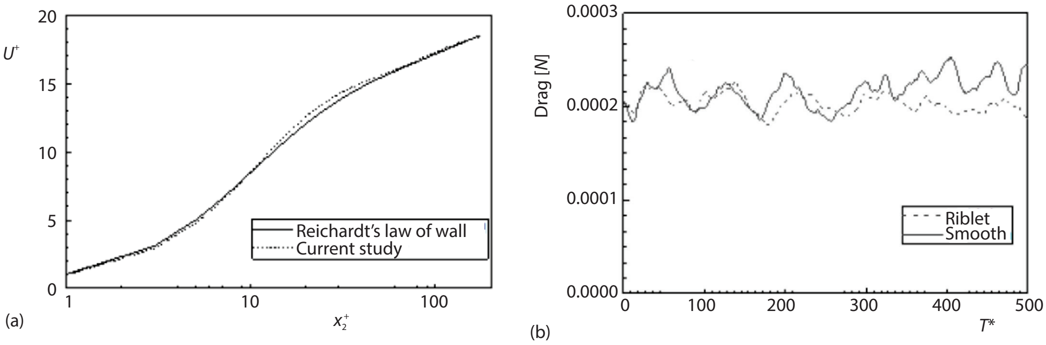

Figure 5. Validation of simulation model at smooth and riblet-structured surface; (a) the streamwise mean velocity profile of flat surface at Re = 4180 is compared against Reichardt's Law of Wall, (b) the drag change over time for both surfaces show quasi-periodic behavior

Based on fig. 5(b), the time-averaged drag value of smooth surface and riblet-structured surface, are 0.000215 N and 0.00020 N, respectively. Comparing the drag change could be evaluated such that:

$$DR\% = \frac{C_{D\mathrm{riblet}} - C_{D\mathrm{smooth}}}{C_{D\mathrm{smooth}}} \tag{15b}$$

The simulation results using the proposed streamlined riblets show drag reduction effect of approximately 7%. The result is in good agreement with the validated numerical result by [22], which reports drag reduction performance of 8.0%. The experimental work by [24] shows drag reduction of 9.0% at riblet height to spacing ratio, h/s = 0.5, which further justify the validity of the drag change in current work, despite slightly broader agreement with current simulated result.

Drag reduction performance of streamlined riblet

In this section, the drag parameters at smooth surface and riblet structured surface are presented for analysis of drag reduction performance by proposed streamlined riblet. The instantaneous drag at both surfaces, D_{smooth} and D_{riblet} are obtained, based on eq. (14). The drag forces are time-averaged over $T^+ = 500$, due to the quasi-periodic behavior of transient simulation in current case. The two-components of total drag force in streamwise direction: frictional drag D_f and pressure drag D_p are investigated, due to the introduction of wetted surface normal to the streamwise direction, $A_{\hat{n}\cdot\hat{t}}$, by streamlined-shaped riblet. The computation of drag coefficients is highly affected by the selection of reference area, since the flow considered in current work neglects the change of density due to incompressibility. The projected area in the normal direction, x_2, to respective surface, $(L \times W)$ is taken as the reference area for computation of drag coefficients for all cases in current work.

Figure 6(a) shows the drag reduction performance of streamlined riblet at various Reynolds numbers. The highest drag reduction performance of streamlined riblet is 7%, which occurs at Re = 4200. Based on fig. 6(a), the drag reduction performances show decreasing trend with increasing Reynolds number. At case of Re = 10000, the streamlined-riblet shows drag increasing effect, with performance of –2.9%. The trends of current results are compared against results from [22, 24], which demonstrated similar trends of drag change by varying Reynolds numbers, with constant riblet height to spacing ratio $h^+/s^+ = 0.5$. The change of drag reduction performance relies heavily on the thickness of the boundary-layers of the flow, since the riblet structures play the role to restrict the interactions of turbulent vortices in the near-wall boundary-layers. It is suggested that as the Reynolds numbers increase, the near-wall layer of flow which consists of drag-promoting vortices is shifted to a lower location than the protrusion height of riblet. Since more vortices at the near-wall region are not lifted-up at increasing flow rate, this explains the decreasing trend of drag reduction performance. Similar trend such that the vortices interacted more actively with the surface grooves at higher Reynolds numbers are reported by [25]. The phenomena can be justified based on fig. 7, whereby vortices are not lifted-up and interact with surface area of valley region of the riblet structures, which in contrast no similar event found in the case of lower Re = 4200. Based on fig. 7, the drag reduction effect of proposed streamlined-riblet is explained by the lower drag encountered at the riblet surface as

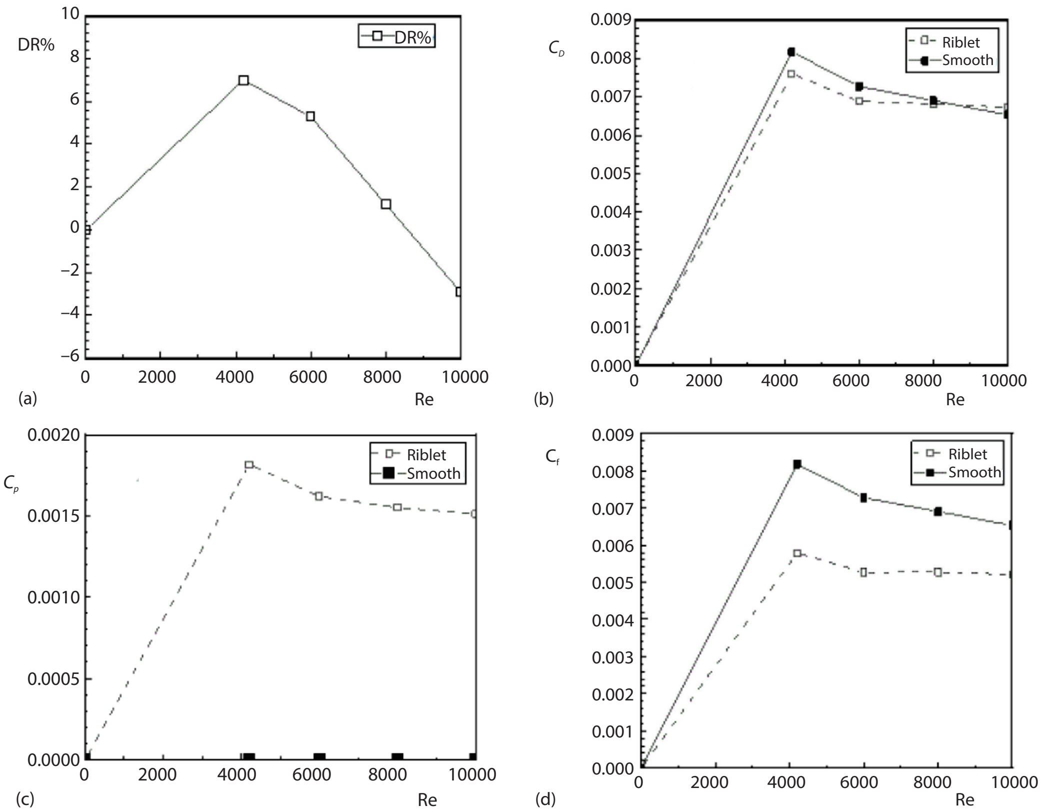

Figure 6. Drag parameters at various Reynolds numbers; (a) drag reduction performance of streamlined-riblet, (b) drag coefficient of riblet and smooth surface, (c) pressure coefficient of riblet and smooth surface, and (d) friction coefficient of riblet and smooth surface

compared to smooth surface due to interactions of vortices with region of small wetted surface area only. This also justifies the capability of proposed surface in maintaining the drag reduction effect of conventional riblets.

Figure 6(b) presents the change of C_D of riblet surface and smooth surface at various Reynolds numbers. Similar to highest drag reduction performance, the highest C_D of streamlined riblet occurs at Re = 4200. The predicted values of C_D show decreasing trend with increasing in Reynolds Number. At case of Re = 10000, the C_D of riblet surface is higher than smooth surface, which explains the drag increasing phenomena at the corresponding case. As compared to smooth surface, the C_D of riblet shows smaller decrease of values as Reynolds numbers increases, this result in the eventual surpass of C_D values of riblets at higher Reynolds numbers. The observed trend suggests that riblet surface is more sensitive towards flow parameters than smooth surface. The change of C_f and C_p of riblet surface and smooth surface at various Reynolds numbers are presented in figs. 6(c) and 6(d), respectively. The C_f of riblet surface and smooth surface decreases across increasing Reynolds numbers. Similar to the trend of C_D, the difference of C_f between riblet and smooth surface becomes smaller with increased Reynolds numbers. This can be due to higher turbulence level at higher Reynolds numbers which causes higher wall shear stress due to stronger interactions of turbulent vortices with the respective surfaces. From here, it is rational to suggest that for drag-increasing case (Re = 10000), the level of interactions of vortices with riblet

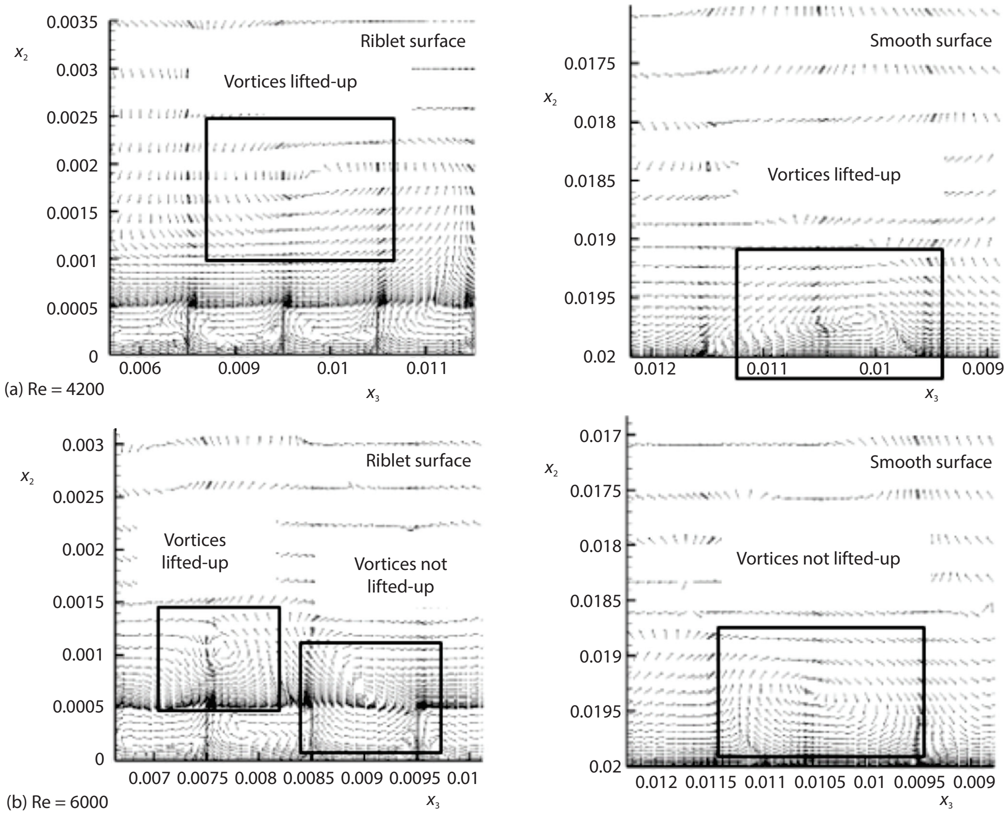

Figure 7. Streamwise vortices for riblet-structured surface and smooth surface at Reynolds number of (a) 4200, (b) 6000; event of drag-inducing vortices not lifted-up happened at increased Reynolds numbers

structures exceeded the level obtained at smooth surface. From fig. 6(d), C_p is reported for case of riblet surface only since there is no normal wetted surface to streamwise direction at the smooth surface. Despite the introduction of pressure drag to the streamlined riblet, the C_p obtained across Reynolds numbers are still relatively smaller than corresponding C_f by magnitude, which result in lower total drag reduction for the drag-reducing cases (Re = 4200, 6000, 8000).

Figure 8 presents the instantaneous wall shear stress encountered by smooth surface and riblet wall. Based on fig. 8(a-i), the wall shear stress at the tips of riblet structures are higher than the rest of the location of riblet surface, which signifies higher drag encountered at tip region of riblet structure. Such phenomenon can be associated with interaction of vortices with riblet tip due to downwash motion from high momentum fluid in the flow. At the smooth surface, the drag encountered is distributed more evenly as compared to riblet surface since there are no geometrical obstacles. From fig. 8(a-ii), the head region of riblet experiences higher drag as compared to tail region of riblet. This can be explained by the experience of pressure drag by the wetted surface area normal to the streamwise flow, and laminarization effect of flow around streamlined-riblet in streamwise direction. The laminarization effect demonstrated by streamlined-riblet will be further discussed in the following section. While the highest drag is encountered at the riblet structure, specifically at the riblet tips, the rest of the region of riblet-structured surface encounters significantly lower drag which gives overall lower surface drag after averaging by surface area, as compared to smooth surface overall drag.

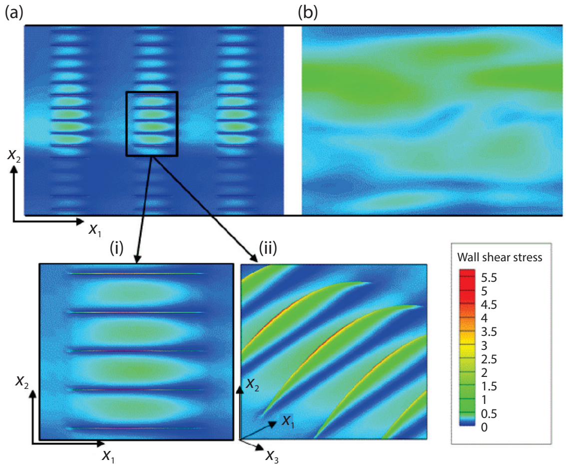

Figure 8. The top view of instantaneous wall shear stress distribution on (a) riblet-structured surface, (b) smooth surface; the enlarged contour distribution from (i) top view and (ii) 3-D view are presented

The presence of riblet structures helps to restrict the interaction of vortices with the viscous flow in the riblet valley, as shown in fig. 7, to ensure low resulted drag at corresponding regions, and leave only high drag to the small area at the riblet tips. Since the total drag encountered at any surface is highly affected by the total wetted surface area, we compare the significance of tangential area by streamlined riblet and *L*-shaped segmented riblet on the resultant drag reduction performances. For fair comparison, the results presented in tab. 2 are obtained from cases with the same flow parameters (Re = 4200), and riblet configuration $h^+/s^+ = 0.5$. Based on tab. 2, the streamlined riblet structure produces higher drag change (7%) as compared to the drag reduction performance obtained by *L*-shaped segmented riblet (3.7%) in the work of [13], under the same flow parameters and geometrical configuration. This suggests that the drag reduction performance of riblet can be optimized from the reduction of wetted surface area. Previously, most studies have been focused on reduction of turbulent drag induced by streamwise vortices, with optimization of height, spacing, and thickness of riblets which often leads to neglect of impact by total wetted surface area. In current work, the streamlined feature has shown its capability to improve the total drag reduction by maintaining the configuration of riblet for restriction of streamwise vortices location while reducing the wetted surface area of riblet for reduction of skin-frictional drag.

Table 2. Comparison of drag reduction performance (DR%) by effect of riblet geometry: (a) effect of $A_{\hat{i}}$ of streamlined riblet on DR%, (b) effect of $A_{\hat{i}}$ of *L*-shaped blade riblet on DR%

<table>
<tr><th>Configurations and dimensions of riblet structure</th><th>Tangential area, $A_{\hat{i}}$ [mm^2]</th><th>DR [%]</th></tr>
<tr><td>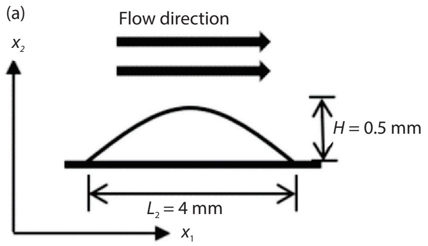
</td><td>$A_{\hat{i}\cdot\hat{i}} = \int_0^4 \left(-\frac{1}{8}L_2^2 + 2L_2\right) dL_2 = 1.33$</td><td>7
Current proposed streamlined riblets</td></tr>
<tr><td>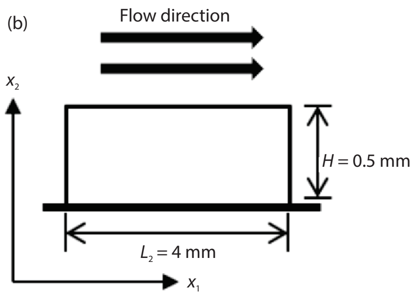
</td><td>$A_{\hat{i}\cdot\hat{i}} = hL_2 = 2$</td><td>3.7 [13]</td></tr>
</table>

Mean streamwise velocity

To relate the drag change at the surfaces to the turbulent dynamics around the riblets, the unsteady mean streamwise velocity profiles is obtained, at varied locations around riblet structure. The results are presented in global co-ordinates, such that the velocities are normalized by predicted centerline velocity, u_o, and wall-normal length is normalized by the channel half-width, δ.

Figure 9 describes the changes of mean streamwise velocity in global co-ordinates at various Reynolds numbers and span-wise locations. For variation of span-wise location, the velocity profiles of riblet tip and valley are compared against the smooth surface. The variation of profiles at varied locations are eminent at the riblet-structured surface as compared to smooth surface, specifically at the near-wall region of $x_2^+ = 0$ to $x_2^+ = 20$. At the region of interest across varied Reynolds numbers, riblet tip shows the highest velocity gradient as compared to riblet valley and smooth surface, while riblet valley has the least velocity gradient. By relating the results to fluid shear stress formula:

$$\tau = \mu \frac{\partial \overline{u}}{\partial x_2} \tag{16}$$

where μ is the denotes dynamic viscosity of fluid, we find higher velocity gradient $\partial \overline{u}/x_2$ increases the drag encountered at the region. This explains why riblet tips encountered highest drag while riblet valleys have the lowest drag, as justified by wall shear stress distribution presented in fig. 8. The findings are in well agreement with previous work on drag reduction by riblet surface [20, 26], such that lower velocity gradient results in lower drag obtained at riblet valley regions.

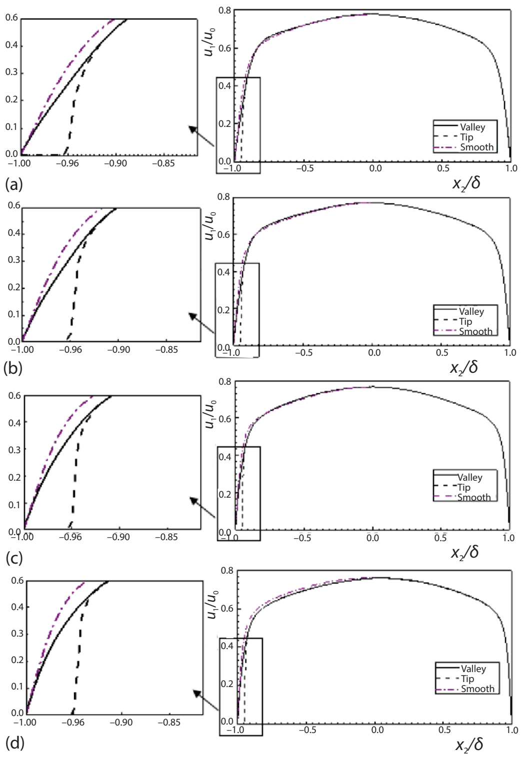

Figure 9. Mean streamwise velocity profile at varied span-wise location; (a) Re = 4200, (b) Re = 6000, (c) Re = 8000, and (d) Re = 10,000; the data presented are normalized with global co-ordinates; Note: the velocity data for smooth surface is reflected symmetrically at $x_2/\delta = 0$ for better visual comparison against velocity data for locations at riblet surface

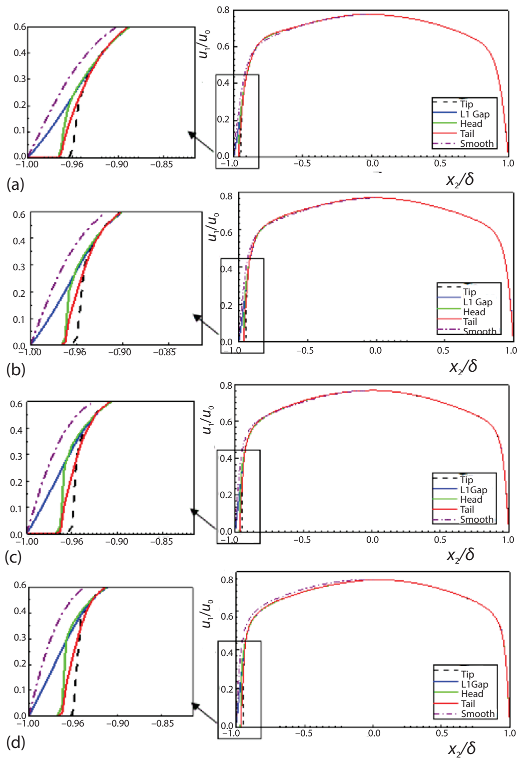

Figure 10. Mean streamwise velocity profile at varied streamwise location; (a) Re = 4200, (b) Re = 6000, (c) Re = 8000, (d) Re = 10000; the presented data are normalized with global co-ordinates; Note: the velocity data for smooth surface is reflected symmetrically at $x_2/\delta = 0$ for better visual comparison against velocity data for locations at riblet surface

In streamwise variation, the velocity profiles of riblet L_1Gap, head, tip and tail are presented in fig. 10 for comparison. Similar to the trend found in span-wise variation, the changes of profiles are obvious at the wall region of $x_2^+ = 0$ to $x_2^+ = 20$. The velocity gradient at varied streamwise locations, in the order of highest to lowest, are: Tip, Head, Tail, L_1Gap. The riblet region with relatively higher surface wetted area, L_1Gap produces significantly lower velocity gradient than smooth surface, which explains the drag reduction effect in cases of Re = 4000, 6000, and 8000.

It is also important to note that similar trend is observed at riblet valley region which has high surface wetted area, based on fig. 9. As the Reynolds number increases, the velocity gradients at all locations increases, which signifies the tendency of the local velocity profile to become turbulent. The trend observed also explains the decrease of drag reduction performance as the Reynolds number increases. The effect of streamlined-feature in producing viscous flow is evident and in good agreement with findings of [14], especially the transformation of high velocity gradient at the head region of riblet structures to lower velocity gradient at the tail region. Such findings support the relatively higher wall shear stress encountered at head region (frontal) of riblet structures as compared to tail region (back), as observed in fig. 8(a-ii).

Conclusions

Large Eddy Simulations were performed at Reynolds numbers of 4200, 6000, 8000, and 10000 to investigate the turbulence structure near the wall by streamlined-riblet structures in a rectangular channel. The validation results revealed good agreement between the simulation results and analytical solution of mean streamwise velocity profile, and capability of predicting drag parameters based on comparison against experimental data. It is shown that streamlined feature of proposed riblet helps in improving the overall drag reduction in the channel flow. Results of drag parameters computed reveal maximum drag reduction performance of around 7%, which is higher than the *L*-shaped segmented riblets with larger wetted surface area, under similar flow and geometrical configurations. It is suggested that the near-wall layers which consists of drag-inducing vortices are shifted to lower locations as the Reynolds number increases, causing interactions of more vortices with the riblet surface since they are not lifted-up, which explains the decrease of drag reduction performance as Reynolds numbers increase. The changes of mean streamwise velocity profile obtained at varied streamwise locations along riblet structures is indicating that streamlined feature helps in lowering the mean velocity gradient, which leads to lower drag achieved at the tail region of riblet structures due to laminarization effect. The mean streamwise velocity data with span-wise variations indicate presence of laminar flow in the valley region due to lower velocity gradient, while tip region has higher velocity gradient which is due to interactions of vortices with the tips. Based on present findings, the streamlined-riblet structure improves the drag reduction performance by possessing lower wetted surface area and lowering velocity gradient of flow due to streamlined feature, while retaining the drag-reducing capabilities of conventional riblet configuration.

Acknowledgment

This work was fully supported and financially funded by Ministry of Higher Education (MOHE) of Malaysia under the project FRGS/1/2017/STG02/UTP/01/1 (CS: 0153AB-L58). The support from Mechanical Engineering Department of Universiti Teknologi PETRONAS in providing the logistic and technical support is highly appreciated.

Compliance with ethical standards

Funding: This study was funded by Ministry of Higher Education (MOHE) of Malaysia (grant number FRGS/1/2017/STG02/UTP/01/1).

Conflict of Interest: The first author, Mr. Desmond has gotten allowances undergraduate Research Assistance (GRA) scheme from Universiti Teknologi PETRONAS which covers his MSc study fees. Also, he received monthly salary from the aforementioned FRGS fund. The second author, Prof Hussain who is the corresponding author, received research grants from Ministry of Higher Education (MOHE) of Malaysia (grant number FRGS/1/2017/STG02/UTP/01/1). The third author, Dr Jundika is contributing to the research as co-supervisor of the first author, Mr. Desmond. The authors declare that they have no conflict of interest.

References

[1] Toms, B. A., Some Observations on the Flow of Linear Polymer Solutions through Straight Tubes at Large Reynolds Numbers, *Proceedings*, 1st International Congress on Rheology, Amsterdam, The Netherlands, 1948, Vol. 2, pp. 135-141
[2] Robinson, S. K., A Review of Vortex Structures and Associated Coherent Motions in Turbulent Boundary-Layers, Eds. A. Gyr, in: *Structure of Turbulence and Drag Reduction. International Union of Theoretical and Applied Mechanics*, Springer-Heidelberg, Berlin 1990, pp. 23-50

[3] Moin, P., Analysis of Turbulence Data Generated by Numerical Simulations, *Proceedings*, 25th AIAA Aerospace Sciences Meeting, Reno, Nev., USA, 1987
[4] Smith, C. R., *et al*., Hairpin Vortices in Turbulent Boundary-Layers: The Implications for Reducing Surface Drag, in Structure of Turbulence and Drag Reduction, *Proceedings*, IUTAM Symposium Zurich, Switzerland, 1990, pp. 51-58
[5] Goldstein, D., *et al*., Direct Numerical Simulation of Turbulent Flow over a Modeled Riblet Covered Surface, *Journal Fluid Mech*., *302* (1995), Nov., pp. 333-376
[6] Dean, B., Bhushan, B., Shark-Skin Surfaces for Fluid-Drag Reduction in Turbulent Flow: A Review, *Philos. Trans. R. Soc. Math. Phys. Eng. Sci*., *368*, (2010), 1929, pp. 4775-4806
[7] Liu, K. N., *et al*., Drag Reduction in Pipes Lined with Riblets, *AIAA J*., *28* (1990), 10, pp 545-551
[8] Chu, D. C., Karniadakis, G. E., A Direct Numerical Simulation of Laminar and Turbulent Flow over Riblet-Mounted Surfaces, *Journal Fluid Mech*., *250* (1993), May, pp. 1-42
[9] Jung, Y. C., Bhushan, B., Biomimetic Structures for Fluid Drag Reduction in Laminar and Turbulent Flows, *Journal Phys. Condens*, *Matter Inst. Phys. J*., *22* (2010), 3, 035104
[10] Walsh, M. J., Weinstein, L. M., Drag and Heat Transfer on Surfaces with Small Longitudinal Fins, *Proceedings*, 11th Fluid and Plasma Dynamics Conference, American Institute of Aeronautics and Astronautics, Seattle, Wash., USA, 1978
[11] Walsh, M. J., Drag Characteristics of V-groove and Transverse Curvature Riblets, Viscose Drag Reduction, *AIAA*, (1980), pp. 168-184
[12] Bechert, D. W., *et al*., Experiments with 3-D Riblets as an Idealized Model of Shark Skin, *Exp. Fluids*, *28* (2000), 5, pp. 403-412
[13] Martin, S., Bhushan, B., Fluid-Flow Analysis of Continuous and Segmented Riblet Structures, *RSC Adv*., *6* (2016), 13, pp. 10962-10978
[14] Bokhorst, E. V., *et al*., Feather Roughness Reduces Flow Separation during Low Reynolds Number Glides of Swifts, *Journal Exp. Biol*., *218* (2015), 20, pp. 3179-3191
[15] Stanković, B. D., *et al*., Specific Aspects of Turbulent Flow in Rectangular Ducts, *Thermal Science*, *21* (2017), Suppl. 3, pp. S663-S678
[16] Smagorinsky, J., General Circulation Experiments with the Primitive Equations, *Mon. Weather Rev.*, *91* (1963), Mar., p. 99
[17] Lilly, D. K., A Proposed Modification of the Germano Subgrid-Scale Closure Method, *Phys. Fluids Fluid Dyn*., *4* (1992) 3, pp. 633-635
[18] Patel, V. C., Head, M. R., Some Observations on Skin Friction and Velocity Profiles in Fully Developed Pipe and Channel Flows, *Journal Fluid Mech*., *38* (1969), 1, pp. 181-201
[19] Jimenez J., Moin, P., The Minimal Flow Unit in Near-Wall Turbulence, *Journal Fluid Mech*., *225* (1991), Apr., pp. 213-240
[20] Choi, H., *et al*., Direct Numerical Simulation of Turbulent Flow over Riblets, *Journal Fluid Mech*., *255* (1993), Oct., pp. 503-539
[21] Russo F., Basse, N. T., Scaling of Turbulence Intensity for Low-Speed Flow in Smooth Pipes, *Flow Meas. Instrum.*, *52* (2016), Dec., pp. 101-114
[22] Martin, S., Bhushan, B., Fluid-Flow Analysis of a Shark-Inspired Microstructure, *Journal Fluid Mech*., *756* (2014), Oct., pp. 5-29
[23] Reichardt, H., Vollständige Darstellung der turbulenten Geschwindigkeitsverteilung in glatten Leitungen, (in German), *ZAMM – J. Appl. Math. Mech. Z. Für Angew. Math. Mech*., *31* (1951), 7, pp. 208-219
[24] Bechert, D., *et al*., Experiments on Drag-Reducing Surfaces and Their Optimization with an Adjustable Geometry, *Journale Fluid Mech*., *338* (1997), May, pp. 59-87
[25] Lee, S.-J., Jang, Y.-G., Control of Flow around a NACA 0012 Airfoil with a Micro-Riblet Film, *Journal Fluids Struct*., *20* (2005), 5, pp. 659-672
[26] Krieger, V., *et al*., Toward Design of the Antiturbulence Surface Exhibiting Maximum Drag Reduction Effect, *Journal Fluid Mech*., *850* (2018), Sept., pp. 262-303

Paper submitted: September 9, 2019
Paper revised: November 25, 2019
Paper accepted: January 27, 2020